Chapter 11
Preparation of Ni-doped ZnO Nanorods by Hydrothermal Route for Gas Sensor Applications

G. H. Jain, G. E. Patil, G. J. Mogal, D. V. Ahire, R. L. Patil, D. D. Kajale, S. D. Shinde and V. B. Gaikwad

Abstract In this work, we propose a novel method for the synthesis Ni-doped ZnO nanorods, analytical grade zinc acetate dehydrate [$Zn(Ac)_2.2H_2O$], nickel acetate [$Ni(Ac)_2.4H_2O$], sodium hydroxide (NaOH) and poly vinyl alcohol (PVA) were used. All the reagents were used as received (Sigma Aldrich, USA) without further purification. Various $(Zn_{1-x}Ni_x)O$ (x = 0.01, 0.06, and 0.10) nanorods were obtained via a facile hydrothermal method. This work aims at preparing sensing material of Ni-doped ZnO nanorods by hydrothermal process, and testing their sensing properties for detection of toxic gases. The growth mechanism, morphology, as well as the gas sensor applications of the Ni-doped ZnO nanorods were systematically studied in this chapter.

Keywords Hydrothermal route · Ni-doped ZnO nanorods · Gas sensor

1 Introduction

Nanostructured ZnO has been widely exploited due to good semiconducting and electronic properties. These properties drive micro device applications such as thin film transistors, high power LED, gas sensors, and spintronic devices [1–4]. Due to

G. H. Jain (✉) · G. E. Patil · G. J. Mogal · D. V. Ahire · R. L. Patil
Materials Research Laboratory, K. T. H. M. College, Nashik 422002, India
e-mail: gotanjain@rediffmail.com

D.D. Kajale
Materials Research Laboratory, Arts, Commerce and Science College, Nandgaon 423106, India

S. D. Shinde
Department of Physics, H. P. T. Arts and R. Y. K. Science College, Nashik 422013, India

V. B. Gaikwad
B. C. U. D, University of Pune, Pune 411007, India

A. Mason et al. (eds.), *Sensing Technology: Current Status and Future Trends I*, Smart Sensors, Measurement and Instrumentation 7, DOI: 10.1007/978-3-319-02318-2_11,

its high surface area, nanostructured ZnO was able to detect the sub ppm range of volatile gases such as acetone and ethanol in gas sensor applications [5, 6]. Room temperature sensing can expand the application of metal oxide based gas sensors to areas such as explosive and flammable gas detection, and the biomedical field [7]. Nevertheless, metal oxide gas sensors are commonly operated at an elevated temperature to overcome the energy required for the chemisorptions between gas molecules, which allows for high sensitivity with a short response time. To overcome the limits of high operating temperature, noble metals such as platinum, palladium, and gold have been doped. This has improved sensing properties at relatively lower temperatures by enhancing interactions between dopants and gas molecules [8–10].

Doping of transition metals in ZnO has been mostly investigated in modifying ferroelectric properties [11–13], but few studies have focused on transition metal doping for enhancing gas sensing properties. Nickel was chosen as a dopant for ZnO nanorods because of similar ionic radius with zinc ions [14] and facile incorporation of Ni into ZnO without altering ZnO morphology.

Solid-state gas sensors make use of the chemical sensitivity of semiconductor surfaces to different adsorbed gases. Appropriate donor doping can produce the electronic defects that increase the influence of oxygen partial pressure on the conductivity. Doped zinc oxide films have a number of attractive applications, such as: gas sensor devices [15], transparent electrodes [16], and piezoelectric devices [17]. Several techniques have been used to produce many distinct zinc oxide films: chemical vapor deposition [18], radio frequency magnetron sputtering [19], sol–gel [20], spray pyrolysis [21–23], hydrothermal [24–28].

The aim of the present chapter is the investigation of structures, optical properties and gas sensing properties of Ni-doped ZnO hexagonal nanorods, which is very important for both fundamental and applied points of view. Furthermore, Ni^{2+} ion with the smaller radius (0.069 nm) compared to Zn^{2+} ion (0.074 nm) is facile to implant the critical nuclei of ZnO during the nano-crystalline growth.

2 Experimental

2.1 Synthesis of ZnO and Ni-doped ZnO Nanorods

ZnO was prepared as per the procedure mentioned in the Chap. 5 and used as it is. For the synthesis of Ni-doped ZnO nanorods, analytical grade zinc acetate dehydrate [$Zn(Ac)_2.2H_2O$], nickel acetate [$Ni(Ac)_2.4H_2O$], sodium hydroxide (NaOH) and poly vinyl alcohol (PVA) were used. All the reagents were used as received (Sigma Aldrich, USA) without further purification. Various $(Zn_{1-x}Ni_x)O$ ($x = 0.01$, 0.06, and 0.10) nanorods were obtained via a facile hydrothermal method. In this, 1 mmol zinc acetate [$Zn(Ac)_2.2H_2O$] and required amount nickel acetate [$Ni(Ac)_2.4H_2O$] were dissolved in absolute ethanol to form a 25 ml

solution. A 3.0 g of PVP were dissolved in 50 ml deionized water and stirred for 30 min. Simultaneously, a 10 ml NaOH (10 M) was added drop wise into this aqueous zinc acetates, nickel nitrate and PVP solution under vigorous stirring. During the addition of NaOH into aqueous solution, the solution was heated at 80 °C to avoid the immediate precipitation of zinc and nickel ions. At last, the final solution was transferred into a 100 ml Teflon-lined stainless steel autoclave. The autoclave was sealed and maintained at 200 °C for 12 h, and then allowed to cool to room temperature naturally. After terminating the reaction in desired time, the resulted solid projects were centrifuged, washed with distilled water and ethanol to remove the ions possibly remaining in the final product, and finally dried in air at 60 °C for 4 h. The synthesized Ni-doped ZnO nanorods were characterized in terms of their structural, optical and gas sensing performances.

2.2 Preparation of Thick Films

The thixotropic paste was formulated by mixing the fine powder of as prepared ZnO and $Zn_{1-x}Ni_xO$ (x = 0.01, 0.06 and 0.10) nanorods with the solution of ethyl cellulose (a temporary binder) in a mixture of organic solvents such as butyl cellulose, butyl carbitol acetate and terpineol etc. The ratio of inorganic part to organic part was kept at 75:25 in formulating the paste. This paste was screen printed [29, 30] on glass substrate in the desired pattern. The films were fired at 550 °C for 30 min.

3 Characterization Results

3.1 X-ray Diffraction Patterns of the ZnO and Ni-doped ZnO Samples

Figure 1 displays X-ray diffraction patterns of the as-prepared ZnO and Ni-doped ZnO samples. The XRD spectra of Ni-doped ZnO rod arrays consist of (100), (002), (101), (102), (110), (103), (200), (112), (201), (004), (202), and (103) peaks, and all the observed diffraction peaks can be indexed to ZnO wurtzite structure. The strong (101) peak proves that ZnO rods with wurtzite structure were obtained in both undoped and Ni-doped ZnO samples. No diffraction peaks of other structures were detected in these samples, indicating that the Ni ion successfully occupied ZnO lattice site and there were no secondary phases or precipitates in the samples. The crystallites sizes of the ZnO and Ni-doped ZnO are estimated using the Scherrer formula. The average values of grain sizes are 27, 23, 15 and 6 nm for the ZnO, $(Zn_{0.99}Ni_{0.01})O$, $(Zn_{0.94}Ni_{0.06})O$, and $(Zn_{0.90}Ni_{0.10})O$ respectively.

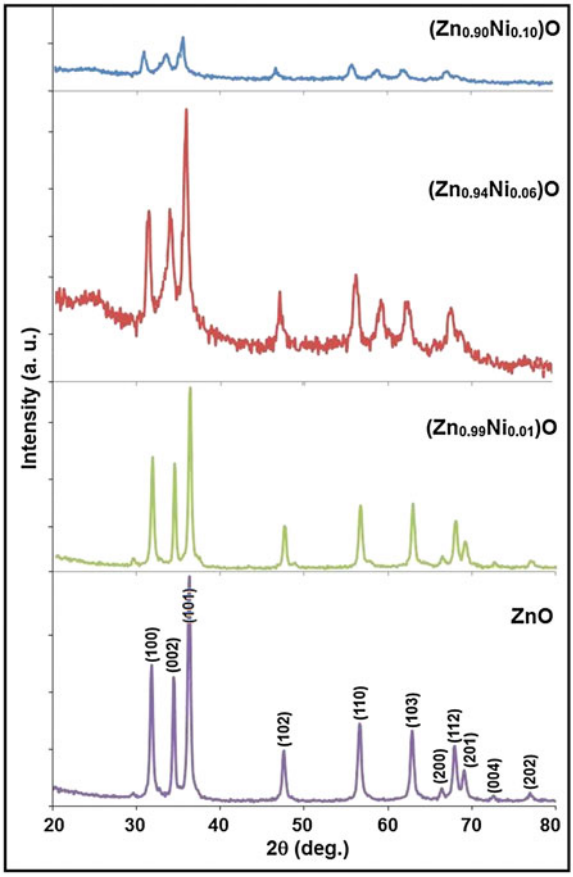

Fig. 1 X-ray diffraction patterns of the ZnO and Ni-doped ZnO samples

The prepared undoped and Ni-doped ZnO were demonstrated to be preferential orientation along the (101) peak direction. The all diffraction peaks of Ni-doped ZnO were obviously higher than that of undoped ZnO. However, $(Zn_{0.99}Ni_{0.01})O$ XRD spectrum has the same height of diffraction peaks as ZnO, which might be due to lower Ni_2^+ concentration. Due to the higher bond energy of Ni^{2+}–O_2^- compared to that of Zn^{2+}–O_2^-, the more energy is required to make Ni^{2+} ions enter into lattice and form the bond of Ni^{2+}–O_2^-.Therefore, of Ni^{2+} substituting for Zn^{2+} has higher stability relative to the Zn–O structure, and more energy is required for the substituted samples to complete crystallization. In addition, because of the larger radius of Zn^{2+} (0.74 Å) [31] compared to Ni^{2+} (0.69 Å), the replacement of Zn^{2+} by Ni^{2+} will cause only slight decrease in lattice parameters. Although doping does not alter the crystal structure, it causes the lattice constant to change as evidence of the (101) peak position shift. Although the change is very little, the concentration of dopant plays a role in the c-axis constant.

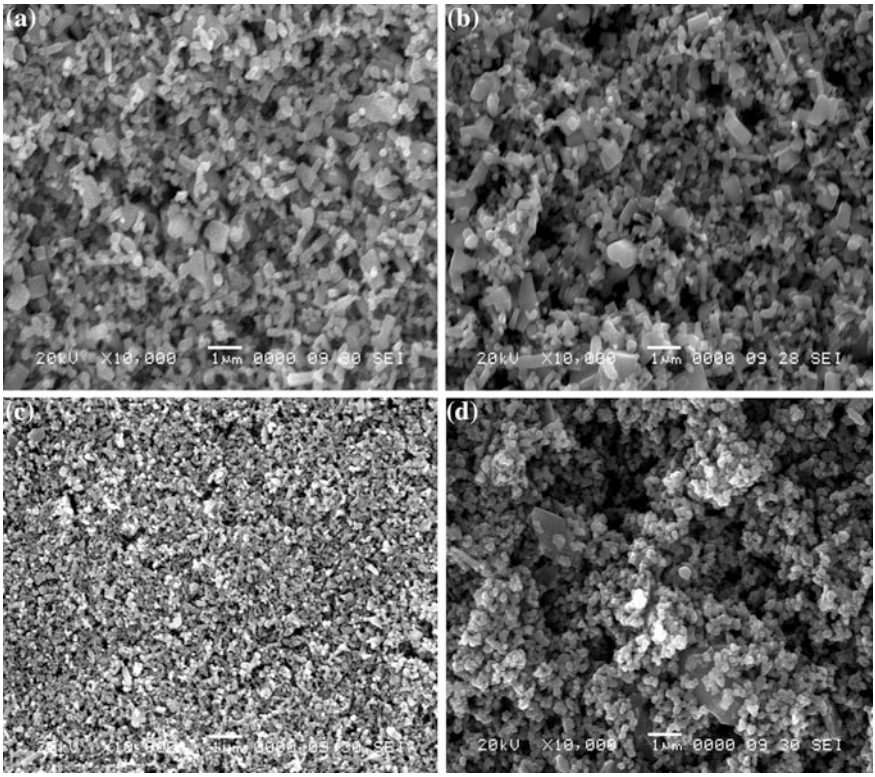

Fig. 2 SEM images of: **a** ZnO, **b** $(Zn_{0.99}Ni_{0.01})O$, **c** $(Zn_{0.94}Ni_{0.04})O$, and **d** $(Zn_{0.90}Ni_{0.10})O$ thick films

The capping ligand, polyvinyl pyrolidone (PVP) was used in the preparation of Ni-doped ZnO nanorods. The PVP can change the surface energy of different crystal facets, the side facets may possess higher energy than the top-down surfaces, and thus ultimately leading to the formation of Ni-doped ZnO nanorods. Matysina [32] determined that hexagonal metals with c/a ratios greater than 1.633 have {101} and {100} surface energy 1.5 times larger than those for {001} facets [33]. Ni-doped ZnO has a c/a ratio of 2.6 and should have even higher surface energy on the {101} and {100} surfaces. As a result, the Ni-doped ZnO nanorods grow more rapidly along these facets and the [110] direction is the long axes of the nanorod while the [001] direction is the short axis. On the other hand, Muthukumar et al. [34] found that the Ni-doped into the ZnO could control the surface morphology by lowering the surface energy. It may be speculated that the Ni element doped into the crystal lattice of the Zn embryos lowers the surface energy of the (10–10) planes, resulting in an isotropic oxidation growth of the Zn embryos instead of the preferred growth at (10–10). At the same time, the completely oxidized embryos may coalesce Ni each other with the definite direction (10–10) and the regularly hexagonal Ni-doped ZnO nanoparticles are synthesized Fig. 2.

Therefore, the formation of the Ni-doped ZnO nanoparticles may be controlled by the Ni-doped into the lattice of the Zn embryos. This is also observed in the XRDs and TEM images of Ni-doped ZnO reported in this work.

4 Transmission Electron Micrograph

Figure. 3a–d shows the TEM and SAED images of (a) ZnO, (b) $(Zn_{0.99}Ni_{0.01})O$, (c) $(Zn_{0.94}Ni_{0.04})O$ and (d) $(Zn_{0.90}Ni_{0.10})O$ powders respectively. The images clearly indicate that the average crystallite size is decreasing with an increase Ni concentrations. The clarity of the rings in the SAED pattern goes on decreasing with Ni-dopant concentration which reveals that the particle sizes of Ni-doped ZnO particles are decreasing. The $(Zn_{0.90}Ni_{0.10})O$ powder shows the diffuse ring pattern which indicates the more decrease in particle size compared with others.

The ZnO rods length ranges from 50 to 120 nm and showing crystalline nature Fig. 3a, while the lengths of rods for $(Zn_{0.99}Ni_{0.01})O$ changes slightly but not remarkably (Fig. 3b). The remarkable decrease in length of the rods was observed in $(Zn_{0.94}Ni_{0.04})O$ and $(Zn_{0.90}Ni_{0.10})O$ powders, Fig. 3c, d. The range of rods length for $(Zn_{0.94}Ni_{0.04})O$ is about 40–80 nm and for $(Zn_{0.90}Ni_{0.10})O$ is about 10–40 nm, with some agglomeration, which might be the reason for decrease in surface area of this powder.

5 Gas Sensing Performance

5.1 Gas Response of ZnO and Ni-doped ZnO Rods

Thick films of ZnO and Ni-doped ZnO nanorods were tested to various gases such as: LPG, CO, CO_2, ethanol, O_2, NH_3, H_2S and Cl_2 etc. at operating temperatures ranging from 25 to 300 °C. The ZnO rods film showed maximum response to H_2S gas at 25 °C (RT) and to ethanol vapors at 300 °C as reported in previous chapter. Ni-doped ZnO rods thick films were tested to various gases at various temperatures from 25(RT) to 300 °C and showed maximum response to H_2S gas for lower gas concentration (1 ppm).

Figure 4 shows the gas response as a function of sensor operating temperature for ZnO and Ni-doped ZnO thick films for H_2S gas in air atmosphere. The response to H_2S gas of Ni-doped ZnO thick films was found to be enhanced with increase in Ni concentrations and decreases for further increase in Ni concentrations as shown in Fig. 4. The lower temperature H_2S gas sensing would be due to nano-crystalline particle sizes of the sensor element, which offers more surfaces to volume ratio causes the oxidation of H_2S gas at room temperature.

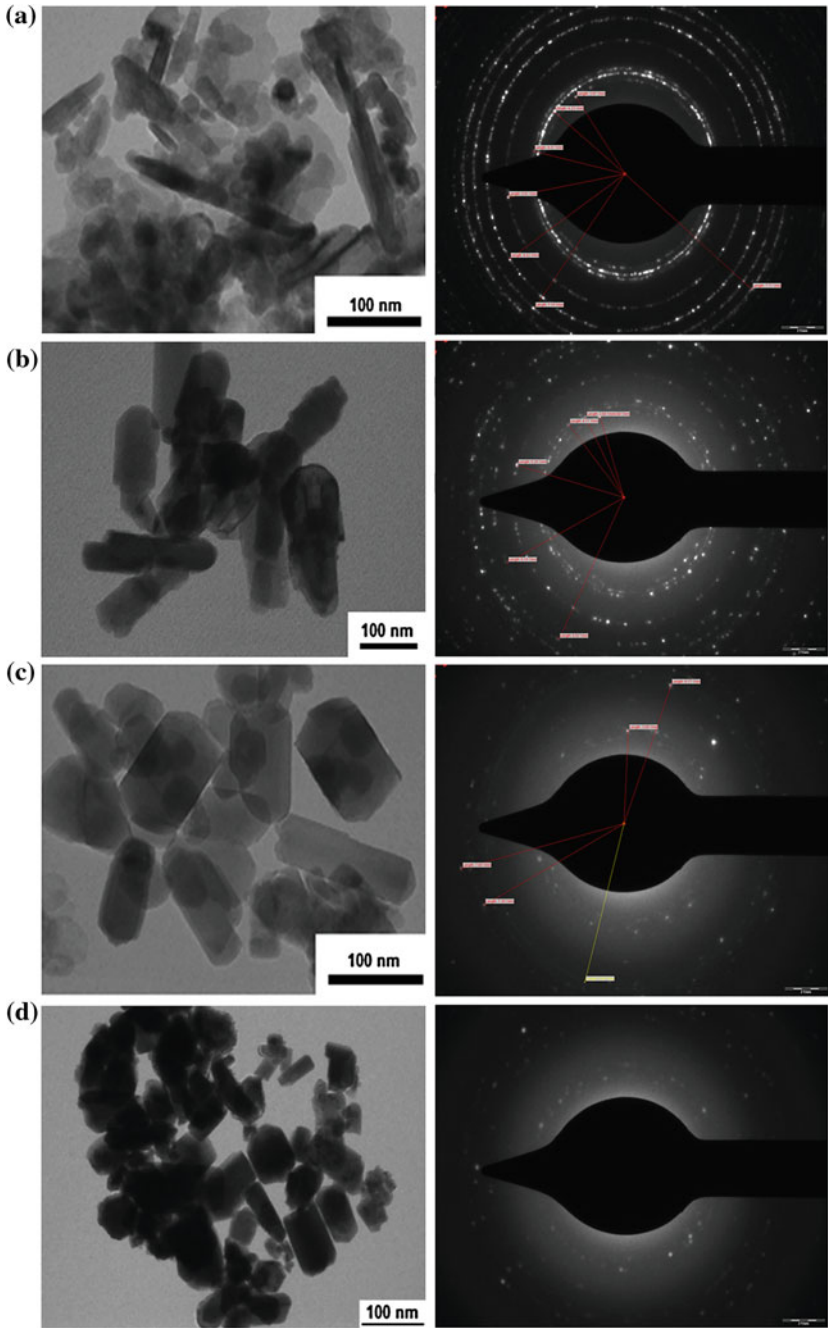

Fig. 3 TEM and SAED images of: **a** ZnO, **b** $(Zn_{0.99}Ni_{0.01})O$, **c** $(Zn_{0.94}Ni_{0.04})O$ and **d** $(Zn_{0.90}Ni_{0.10})O$ powders respectively

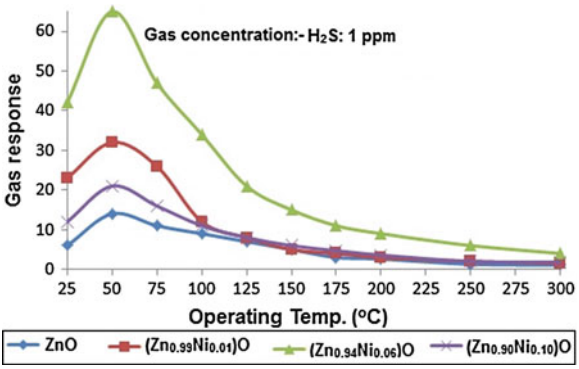

Fig. 4 Variation of H_2S gas response with operating temperature

From Fig. 4 H_2S gas response increases with operating temperature, attains maximum at 50 °C and decreases with further increases in temperature. But the sensor has potential to detect H_2S gas at lower temperature 25 °C (RT).

5.2 Selectivity of ZnO and Ni-doped ZnO Rods Thick Films

The selectivity is the important feature of the gas sensor. The Fig. 5 shows the bar diagram of the selectivity of the ZnO and Ni-doped ZnO thick films sensor to H_2S gas against the other interfering gases. Thick films of ZnO and Ni-doped ZnO nanorods showed maximum selectivity to H_2S gas against the other gases. The $(Zn_{0.94}Ni_{0.06})O$ thick film was found to be most selective to H_2S gas compared to the other gases Fig. 6.

5.3 Response and Recovery Time

The Table 1 shows the response and recovery times of the ZnO and Ni-doped ZnO thick film sensors. The response time of ZnO sensor was quick but comparatively its response is less ($S = 6$) and recovery time was more. But the Ni-doped ZnO sensors showed improved response values but recovery time was more. This would be due to more response values and the energy required to oxidize the H_2S gas was less at lower operating temperature (25 °C). But the $(Zn_{0.94}Ni_{0.04})O$ based sensor has quick response and speedy recovery and showed high response ($S = 42$). This sample has potential to satisfy all sensor specifications requirements.

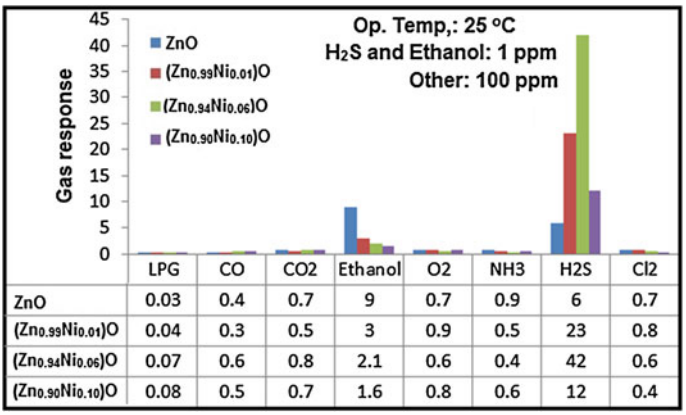

	LPG	CO	CO2	Ethanol	O2	NH3	H2S	Cl2
ZnO	0.03	0.4	0.7	9	0.7	0.9	6	0.7
$(Zn_{0.99}Ni_{0.01})O$	0.04	0.3	0.5	3	0.9	0.5	23	0.8
$(Zn_{0.94}Ni_{0.06})O$	0.07	0.6	0.8	2.1	0.6	0.4	42	0.6
$(Zn_{0.90}Ni_{0.10})O$	0.08	0.5	0.7	1.6	0.8	0.6	12	0.4

Fig. 5 Selectivity of the ZnO and Ni-doped ZnO thick films sensor to H_2S gas at 25 °C (RT)

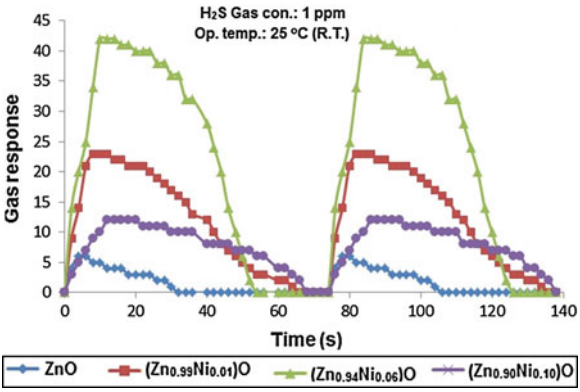

Fig. 6 Response and recovery times of the ZnO and Ni-doped ZnO thick films sensor to H_2S gas at 25 °C (RT)

Table 1 Response and recovery times of the ZnO and Ni-doped ZnO thick film sensors

Samples	Response time	Recovery time
ZnO rods	3 s	24 s
$(Zn_{0.99}Ni_{0.01})O$	8 s	44 s
$(Zn_{0.94}Ni_{0.04})O$	6 s	40 s

5.4 Gas Sensing Mechanism

When reducing gas such as H_2S is inleted, the interaction of this gas with the surface chemisorbed oxygen, O_2^-, can take place. The reducing gas readily releasing electrons back to the conduction band and the electrical conductance of the semiconductor increases.

$$2H_2S + 3O_2^-(ads) \rightarrow 2SO_2(g) + 2H_2O(g) + 6e^- \quad (1)$$

As per earlier reports by many authors, the liberation of water saturates the surface and unless desorbed completely, affects the response of the surface. And hence, after each measurement, the chamber was flushed thoroughly and the sensor was heated to overcome the effect of humidity. But in this experiment, we observed that, this was not essential for these samples. The reason may be due to nonstoichiometry, lattice distortion, smaller grain size, and highest surface activity, which result in stronger interaction between H_2S molecules and the surface active sites [35]. The manifestation of the maximum response at optimal operating temperature is also allied to the formation of charged oxygen ions on the oxide surface. It is possible that Ni-doping not only decreases the particle size but also increases the catalytic activities of the powder. The decrease in particle with optimum Ni-doping is due to the dispersion of the crystallites avoiding the agglomeration. One of the probable explanations for shift in optimal operating temperature towards lower side by 25 °C may be the reduction in the particle size with doping concentration. This can be explained as: in nano-sized particles surface-to-bulk ratio is much larger than that of coarse micro-grained materials, which yields a large interface between the oxide and the gaseous medium. The larger surface area generally provides more adsorption–desorption sites, which can enhance the reactivity at lower temperature. However, the improved response of a nanostructured gas sensor cannot be explained only by reference to the increase in the specific reactive surface; the full depletion of the metal oxide semiconductor as the nanoparticles size approaches the thickness of the space charge region is also important. In a semiconductor metal oxide with grains of diameter D, each grain has an electron-depleted surface layer, also known as the space-charge layer of the depth L [36]. The depth of this layer is determined by both the Debye length of the material and the strength of oxygen chemisorption. The reduction in the grain size allows the space charge to cover large volume of the grain and the large number of grain boundaries and periphery, hence, large variation in the barrier resistance, which helps to significantly enhance gas detection [37–39]. Furthermore, the size-dependent gas-sensing properties are linked to the density of surface states induced by the chemisorbed oxygen species which leads to a lower degree of Fermi level pinning [40]. So the other possibility may be the Fermi level pinning, which may reduce with doping. The Fermi level pinning can help in lowering the temperature and less Fermi level pinning can help in lowering the temperature and less Fermi level pinning means that the surface barrier and accordingly, the overall resistance, can undergo large variations [41]. This may lead to the response of Ni-doped ZnO sensor elements fabricated from nanosized particles with lowering in the optimal operating temperature.

6 Conclusions

From this work, the following conclusions can be drawn:

- The Ni ion successfully occupied ZnO lattice site and there were no secondary phases or precipitates in the samples.
- The size of ZnO decreases with the Ni-concentrations in ZnO and is confirmed by XRD and TEM analysis.
- The response to H_2S gas increases with Ni-dopant concentrations attains maximum and decreases on further increase in dopant concentrations.
- The improvement in H_2S gas response is due to increase in the surface to volume ratio of the Ni-doped ZnO samples.
- The response and recovery times of Ni-doped ZnO samples were quick and fast compared to pure ZnO.
- The $(Zn_{0.94}Ni_{0.6})O$ thick film showed maximum response to H_2S with fast response and recovery time characteristics.

Acknowledgments The author (GHJ) is grateful to U. G. C., New Delhi and BCUD, University of Pune for financial assistance to this project. Authors are very much thankful to Principal, Arts, Commerce and Science College, Nandgaon and Principal, K. T. H. M College, Nashik for providing experimental facilities.

References

1. P.F. Carcia, R.S. McLean, G. Nunes, Transparent ZnO thin-film transistor fabricated by rf magnetron sputtering. Appl. Phys. Lett. **82**, 1117–1120 (2003)
2. J.H. Lim, C.K. Kang, K.K. Kim, I.K. Park, D.K. Hwang, S.J. Park, UV electroluminescence emission from ZnO light-emitting diodes grown by high temperature radiofrequency sputtering. Adv. Mater. **18**(20), 2720–2724 (2006)
3. H.-U. Lee, Kyun Ahn, S.-J. Lee, J.-P. Kim, H.-G. Kim, S.-Y. Jeong, C.-R. Cho, ZnO nanobarbed fibers: fabrication, sensing NO_2 gas, and their sensing mechanism. Appl. Phys. Lett. **98**, 193114–193116 (2011)
4. C. Ronning, Manganese-doped ZnO nanobelts for spintronics. Appl. Phys. Lett. **84**, 783–785 (2004)
5. Q. Wan, Fabrication and ethanol sensing characteristics of ZnO nanowire gas sensors. Appl. Phys. Lett. **84**, 3654–3656 (2004)
6. Q. Qi, Selective acetone sensor based on dumbbell-like. ZnO with rapid response and recovery. Sens. Actuators B Chem. **134**, 166–170 (2008)
7. L.Y. Zhang, L.W. Yin, C.X. Wang, N. Lun, Y.X. Qi, D. Xiang, Origin of visible photoluminescence of ZnO quantum dots: defect-dependent and size-dependent. J. Phys. Chem. **114**, 9651–9658 (2010)
8. Z. Zhou, K. Kato, T. Komaki, M. Yoshino, H. Yukawa, M. Morinaga, K. Morita, Effects of dopants and hydrogen on the electrical conductivity of ZnO. J. Europian Ceram. Soc. **24**, 139–146 (2004)
9. N. Hongsith, C. Viriyaworasakul, S. Choopun, Ethanol sensor based on ZnO and Au-doped ZnO nanowires. Ceram. Int. **34**, 823–826 (2008)

10. J.K. Song, J.M. Szarko, S.R. Leone, S.H. Li, Y.P. Zhao, Ultrafast carrier dynamics and wavelength-dependent lasing-time characteristics in single ZnO nanotetrapod and nanowire lasers. J. Phys. Chem. B **109**, 15749–15753 (2005)
11. C. Cheng, G. Xu, H. Zhang, Y. Luo, Hydrothermal synthesis Ni-doped ZnO nanorods with room-temperature ferromagnetism. Mater. Lett. **62**, 1617–1620 (2008)
12. G. Huang, Synthesis, structure, and room-temperature ferromagnetism of Ni-doped ZnO nanoparticles. J. Mater. Sci. **42**, 6464–6468 (2007)
13. H. Wang, ZnO-based light-emitting metal-insulator-semiconductor diodes. Appl. Phys. Lett. **90**, 0525–0527 (2007)
14. R. Shannon, Revised effective ionic radii and systematic studies of interatomic distances in halides and chalcogenides. Acta Crystallogr. A **32**, 751–767 (1976)
15. C.H. Kwon, H.K. Hong, D.H. Yun, K. Lee, S.T. Kim, Y.H. Roh, B.H. Lee, Thick-film zinc-oxide gas sensor for the control of lean air-to-fuel ratio in domestic combustion systems. Sens. Actuators B Chem **24**, 610–613 (1995)
16. S. Major, S. Kumar, M. Bhatnagar, K.L. Chopra, Effect of hydrogen plasma treatment on transparent conducting oxides. Appl. Phys. Lett. **49**, 394–396 (1986)
17. M.G. Ambia, M.N. Islam, M. Obaidul Hakim, Studies on the seebeck effect in semiconducting ZnO thin films. J. Mater. Sci. **27**, 5169–5176 (1992)
18. J. Hu, R.G. Gordon, Textured aluminum-doped zinc oxide thin films from atmospheric pressure chemical-vapor deposition. J. Appl. Phys. **71**, 880–884 (1992)
19. O. Takai, M. Futsuhara, G. Shimizu, C.P. Lungu, J. Nozue, Nanostructure of ZnO thin films prepared by reactive rf magnetron sputtering. Thin Solid Films **318**, 117–119 (1998)
20. M. Ohyama, H. Kozuka, T. Yoko, Sol-gel preparation of ZnO films with extremely preferred orientation along (002) plane from zinc acetate solution. Thin Solid Films **306**, 78–85 (1997)
21. S.D. Shinde, G.E. Patil, D.D. Kajale, V.B. Gaikwad, G.H. Jain, Synthesis of ZnO nanorods by spray pyrolysis for H_2S gas sensor. J. Alloy. Compd. **528**, 109–114 (2012)
22. G.E Patil, D.D. Kajale, P.T. Ahire, D.N. Chavan, N.K. Pawar, S.D. Shinde, V.B. Gaikwad, G.H. Jain, Synthesis, characterization and gas sensing performance of SnO_2 thin films prepared by spray pyrolysis. Bull. Mater. Sci. **34,** 1–9 (2011)
23. G.E. Patil, D.D. Kajale, V.B. Gaikwad, G.H. Jain, Effect of thickness on nanostructured SnO_2 thin films by spray pyrolysis as highly sensitive H_2S gas sensor. Adv. Sci. Lett. **18**, 199–207 (2012)
24. F. Paraguay, W. Estrada, D.R. Acosta, E. Andrade, M. Miki-Yoshida, Growth, structure and optical characterization of high quality ZnO thin films obtained by spray pyrolysis. Thin Solid Films **350**, 192–202 (1999)
25. S.D. Shinde, G.E. Patil, D.D. Kajale, V.B. Gaikwad, G.H. Jain, Synthesis of ZnO nanorods by hydrothermal method for gas sensor applications. Int. J. Smart Sens. Intell. Syst. **5**, 57–70 (2012)
26. S.D. Shinde, G.E. Patil, D.D. Kajale, V.B. Gaikwad, G.H. Jain, Gas sensing performance of nanostructured ZnO thick film resistors. Int. J. Nanoparticles **5**, 126–135 (2012)
27. Y. Zuo, S. Ge, Z.Q. Chen, L. Zhang, X.Y. Zhou, S. Yan, Morphology, optical and magnetic properties of $Zn_{1-x}Ni_xO$ nanorod arrays fabricated by hydrothermal method. J. Alloy. Compd. **470**, 47–50 (2009)
28. T. Al-Harbi, Hydrothermal synthesis and optical properties of Ni doped ZnO hexagonal nanodiscs. J. Alloy. Compd. **509**, 387–390 (2011)
29. G.H. Jain, L.A. Patil, M.S. Wagh, D.R. Patil, S.A. Patil, D.P. Amalnerkar, Surface modified $BaTiO_3$ thick film resistors as H_2S gas sensors. Sens Actuators B Chem **117**, 159–165 (2006)
30. G.H. Jain, L.A. Patil, Gas sensing properties of Cu and Cr activated BST thick films. Bull. Mater. Sci. **29**, 403–411 (2006)
31. R. Viswanatha, S. Sapra, B. Satpati, Synthesis and characterization of Mn-doped ZnO nanocrystals. J. Phys. Chem. B **108**, 6303–6310 (2004)
32. Q.H. Li, Q.Y. Wang, X. Liang, T.H. Wang, Electronic transport through individual ZnO nanowires. Appl. Phys. Lett. **84**, 4556–4560 (2004)

33. A.C. Wang, J.Y. Dai, J.Z. Cheng, M.P. Chudzik, T.J. Marks, R.P.H. Chang, C.R. Kannewurf, Charge transport, optical transparency, microstructure, and processing relationships in transparent conductive indium–zinc oxide films grown by low-pressure metal-organic chemical vapor deposition. Appl. Phys. Lett. **73**, 327–329 (1998)
34. K.R. Kittilstved, N.S. Norberg, D.R. Gamelin, Chemical manipulation of high-Tc ferromagnetism in ZnO diluted magnetic semiconductors. Phys. Rev. Lett. **94**, 1472–1475 (2005)
35. N. Xinshu, Z. Haoxiang, W. Xinjun, J. Kai, Sensing properties of rare earth oxide doped In2O3 by a sol–gel method. Sens. Actuators B Chem. **115**, 434–438 (2006)
36. C. Xu, J. Tamaki, N. Miura, N. Yamazoe, Grain size effects on gas sensitivity of porous SnO_2-based elements. Sens. Actuators B Chem. **3**, 147–155 (1991)
37. P. Serrini, V. Briois, M.C. Horrillo, A. Traverse, L. Manes, Chemical composition and crystalline structure of SnO_2 thin films used as gas sensors. Thin Solid Films **304**, 113–122 (1997)
38. A. Galkidas, A. Mironas, A. Setkus, Peculiarities of surface doping with Cu in SnO_2 thin film gas sensors. Sens. Actuators B Chem. **26**, 29–33 (1995)
39. Q. Pan, J. Xu, X. Dong, J. Xang, Gas-sensitive properties of nanometer-sized SnO_2. Sens. Actuators B Chem. **66**, 237–239 (2000)
40. G.E. Patil, D.D. Kajale, S.D. Shinde, V.G. Wagh, V.B. Gaikwad, G.H. Jain, Synthesis of Cu-Doped SnO_2 thin films by spray pyrolysis for gas sensor application. Adv. Sens. Technol. Smart Sens. Measurement Instrum. **1**, 299–311 (2013)
41. D.D. Kajale, G.E. Patil, V.B. Gaikwad, S.D. Shinde, D.N. Chavan, N.K. Pawar, S.R. Shirsath, G.H. Jain, Synthesis of $SrTiO_3$ nanopowder by sol-gel hydrothermal method for gas sensing application. Int. J. Smart Sens. Intell. Syst. **5**(2), 382–400 (2012)